Influence of wheel speed and ageing on nanostructure and magnetic properties of Cr-doped MnBi magnetic material

Kritika Anand[1,2] · **Nithya Christopher**[1,2] · **Nidhi Singh**[1,2]

Abstract

In the present work, $Mn_{47}Bi_{50}Cr_3$ ribbons were synthesised employing melt spinning at different wheel speeds ranging from 16 to 28 m/s, to study the effect of quenching rate on the microstructure, morphology and magnetic properties of rapidly solidified alloy. X-ray diffraction studies indicate that the FWHM of diffraction peaks for MnBi increases with the increase in wheel speed, leading to a concurrent decrease in the mean grain size. This could be attributed to the high cooling rate causing homogeneous nucleation leading to refined grain size. The maximum value of coercivity of 11.9 kOe and saturation magnetisation of 54.2 emu/g was obtained for the alloy melt spun at 20 m/s, indicating dependence of coercivity on the grain size, and its orientation, which is largely controlled by the wheel speed. Also, XRD pattern confirms that the MnBi phase fraction is found to be maximum at this wheel speed. Therefore, high-performance nanocrystalline $Mn_{47}Bi_{50}Cr_3$ magnetic material has been synthesised by adjusting the wheel speed and thereby tuning the quench rate. In addition, the phase transformation and variation with respect to temperature and time were studied using thermal analysis technique. Stability of magnetic properties of the alloy with respect to time was also studied after the ageing process.

1 Introduction

Research worldwide in the area of permanent magnet is primarily centred around the development of rare-earth free permanent magnet materials due to the environmental and the economical issues hovering over the rare-earth metals [1–3]. The intermetallic alloy MnBi in its low-temperature phase (LTP) has long been a material of interest as it exhibits its hard ferromagnetic properties. At high temperatures, LTP-MnBi displays high coercivity, which is comparable to that of $Nd_2Fe_{14}B$ magnet, thus making it an ideal candidate for high-temperature applications [4]. However, there are issues concerning this material; for example, upon heating beyond 628 K, LTP-MnBi decomposes into high-temperature $Mn_{1.08}Bi$ phase and liquid Bi. Also, MnBi is highly susceptible to oxygen and moisture [5]. In addition to that,

it is difficult to prepare single-phase MnBi by conventional synthesis techniques such as arc melting, melt spinning and sintering, because of the peritectic reaction that occurs at a relatively low temperature. It has been reported that synthesis of more than 90% of LTP-MnBi phase has been possible only by melt spinning method [6]. Kim et al. most recently reported ~98% pure LTP phase for an annealed partially amorphous off-stoichiometric $Mn_{55}Bi_{45}$ alloy synthesised via melt spinning technique [7].

Melt spinning is a widely used technique, primarily employed to produce high-performance permanent magnets by rapid quenching. In this method, rapid cooling of the material occurs during solidification process [8, 9]. The thermal energy dissipated during cooling comprises of both superheat and latent heat. The contact time of liquid metal to the water-cooled rotating wheel is less than a millisecond, leading to a rapid solidification process [10]. Several factors, such as atmosphere inside melt spinning chamber, gas ejection pressure, speed of the rotating wheel, distance between wheel surface and crucible slit, melt superheat, shape and width of crucible slit and the temperature and cooling conditions of copper wheel, influence the cooling behaviour, structure and properties of the rapidly quenched ribbons [10,

✉ Nidhi Singh
 singhnidhi@nplindia.org

1 Academy of Scientific and Innovative Research (AcSIR), Ghaziabad 201002, India

2 CSIR-National Physical Laboratory, Dr. K.S Krishnan Marg, New Delhi 110012, India

11]. Among all these parameters, the wheel speed is the most crucial parameter. Experimentally, the challenge is to thoroughly understand the processing parameters to obtain a homogeneous microstructure and desired properties.

It is a known fact that magnetic properties of MnBi-based materials are strongly dependent on the microstructure, especially grain size and phase distribution [12]. Rama Rao et al. reported an increase in coercivity of MnBi alloy due to decrease in particle size achieved via jet milling [13]. Similar studies have been done by processing the melt at different wheel speeds, giving rise to different cooling rates, thereby resulting in different ribbon thicknesses. This leads to the alterations in the microstructure of the as-spun ribbons and consequently influences the magnetic properties of material [14]. Melt spinning offers a plethora of advantages, but the complexity with this technique lies in the narrow processing window at an optimum wheel speed. Thus, a thorough understanding of melt spinning process parameters and a thoughtful optimisation are necessary to utilise it to its full potential.

The potential of melt spinning and the scope of optimising various process parameters associated have been explored in the present work. The effect of the wheel speed was studied for the alloy of composition $Mn_{47}Bi_{50}Cr_3$. As reported in our previous work, Cr-doped MnBi leads to the decoupling of structural and magnetic transformation temperature, leading to the formation of a more stable LTP-MnBi [15]. An attempt has been made to understand qualitatively the effect of melt spinning parameters, specifically wheel speed on the structural, microstructural, thermal and magnetic properties of $Mn_{47}Bi_{50}Cr_3$ alloy. It was established that the optimised wheel speed is essential to obtain a desired phase structure that promotes high coercivity and a high magnetisation thereby leading to a high figure of merit (BH_{max}).

Additionally, since MnBi alloys are prone to oxygen and moisture, a detailed investigation has been carried out to study the degradation and evolution of LTP-MnBi phase. This is an important study as the oxygen sensitivity as well as the thermal and time stability of LTP-MnBi could be next hindrance for real application of this permanent magnet material.

2 Experimental details

An alloy of composition $Mn_{47}Bi_{50}Cr_3$ was prepared by arc melting, where the constituent elements of purity better than 99.99% were weighed in the stoichiometric ratios and were arc-melted in a mini-arc melter (MAM-1, Edmund Buhler GmbH). The ingots were flipped and re-melted several times to ensure homogeneity. The arcmelted ingots were then melt spun at various wheel speeds in the range of 16 to 28 m/s using melt spinning unit (Melt Spinner HV,

Edmund Buhler GmbH) in order to form nanocrystalline ribbons, keeping rest all the parameters same.

The thickness of the ribbons thus obtained is measured with the digital micrometer (Mitutoyo, least count: 0.001 mm). Structural characterisation was done by X-ray diffraction (XRD) measurement performed in a Rigaku diffractometer using Cu-kα radiation to determine the phase formation. Thermal analysis was carried out using differential scanning calorimeter (DSC, 404 F3 Pegasus, Netzsch), to determine the phase transformation temperatures. The microstructure of the alloy was studied by scanning electron microscope (SEM, EVO MA10). The magnetic properties were measured by the vibrating sample magnetometer (VSM, Lakeshore VSM-7410), up to a maximum field of 2 T.

3 Results and discussion

3.1 Effect of wheel speed on ribbon thickness

The average thickness of as-melt-spun ribbon as a function of varying wheel speed is shown in Fig. 1. The thickness of the ribbon decreases from 59 to 39 μm for the ribbon melt spun at 16 m/s to 28 m/s. The regression analysis was performed to fit the curve with a correlation factor (R^2) of 0.986, which emphasises that the ribbon thickness varies inversely with the wheel speed. The increasing wheel speed leads to the increase in centrifugal force, resulting in the formation of thinner ribbons [16, 17]. Since cooling rate is directly proportional to wheel speed, it can be concluded that ribbon thickness decreases with cooling rate [18].
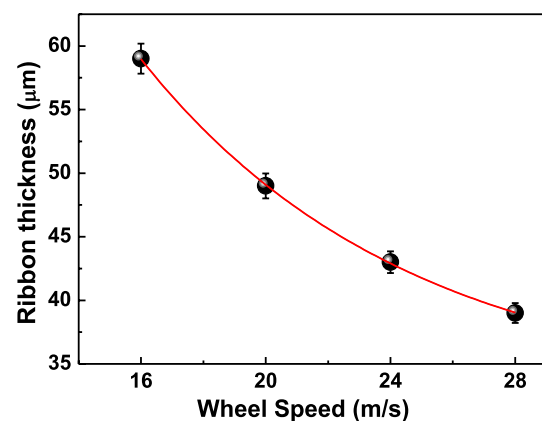
The rate of cooling is given by the equation:

Fig. 1 Effect of variation of wheel speed in melt spinning technique on the thickness of the ribbons of $Mn_{47}Bi_{50}Cr_3$

$$R = \frac{nh(T - T_w)}{c_p \rho d} \qquad (1)$$

where n is the form factor, h represents the heat transfer coefficient, T is the melting temperature, T_w is the temperature of copper wheel, C_p is the latent heat per unit mass, ρ is the density of the material and d is the thickness of the ribbon. This clearly implies that thickness of the ribbon is inversely proportional to the cooling rate and in turn the wheel speed.

3.2 Thermal analysis and effect of ageing

DSC curve for the samples melt spun at different wheel speed is shown in Fig. 2a. As can be seen from the figure, peak at 144 °C is the ferrimagnetic reorganisation temperature, which depicts the small fraction of ferrimagnetic MnBi present in the sample. Peak at 267 °C corresponds to the melting point of bismuth and is due to the reaction from αMnBi + Bi solid, melting to Bi-rich liquid and αMnBi [19]. The third endothermic peak at 359 °C is the LTP-HTP transformation temperature, wherein conversion of αMnBi to βMnBi and the separation of Bi-rich liquid occur. And, finally the peak at 457 °C corresponds to the peritectic reaction of MnBi, where βMnBi transforms to αMn and Bi-rich liquid [20]. A point worth emphasising is that the onset temperature of LTP-HTP transition for all the ribbons is same, which supports the uniformity of phase composition for all ribbons. The difference lies in the enthalpy of crystallisation (ΔH) calculated from the area under the curve, which was observed to increase with the increasing wheel speed. ΔH values for sample melt spun at 16, 20, 24 and 28 m/s was determined to be 1.829, 2.569, 3.681 and 3.71 J/g,

respectively. This clearly implies that the enthalpy of crystallisation depends upon the rate of cooling, and optimised wheel speed is therefore necessary for the formation of a stable alloy [21].

To study the effect of ageing, thermal analysis was carried out on samples kept at ambient conditions for 12 months as shown in Fig. 2b. The effect of oxidation is observed on normalised heat flow curves on all the samples except for sample melt spun at 20 m/s. After ageing in air, only the melting of Bi-rich liquid (at 267 °C) stays well preserved in all the samples, contrary to the MnBi transformations. The broad peak around 222 °C can be regarded as the reaction of thermally unstable oxides, like MnO_2 [22]. The missing LTP-HTP conversion peak indicates the degradation of the majority of LTP-MnBi. Similar effect has been described in [5], where the impact of oxidation on the sample prepared in Ar atmosphere has been studied. Another interesting feature worth emphasising is that the DSC curves of sample melt spun at 20 m/s indicate an absence of oxidation peak at 222 °C, even after 12 months of ageing. The presence of LTP-HTP peak implies that the LTP-MnBi is still preserved. This clearly indicates that the sample melt spun at 20 m/s is more stable than its counterparts and exhibits superior properties.

3.3 Phase analysis

Figure 3a shows the X-ray diffraction pattern of $Mn_{47}Bi_{50}Cr_3$ melt spun at different wheel speed of 16 m/s, 20 m/s, 24 m/s and 28 m/s. LTP-MnBi phase with the 100% peak intensity at 28.3 degrees decreases with the increasing wheel speed, except for the sample melt spun at 20 m/s. This further establishes that the most stable LTP-MnBi was formed at a wheel speed of 20 m/s. Figure 3b shows the XRD pattern
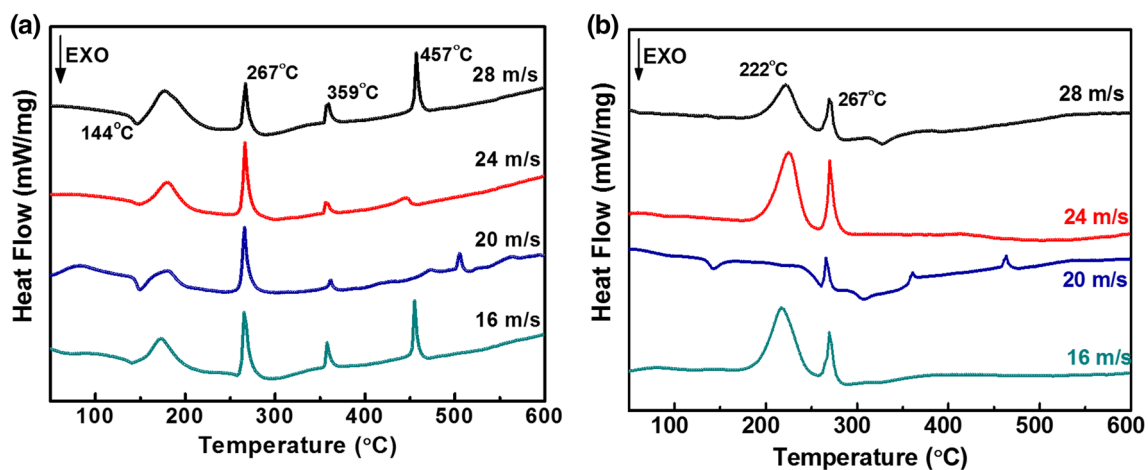

Fig. 2 DSC micrograph of $Mn_{47}Bi_{50}Cr_3$ melt-spun ribbons at various wheel speeds of 16 m/s, 20 m/s, 24 m/s 28 m/s: **a** as-prepared sample, **b** sample aged for 12 months, measured under the similar conditions
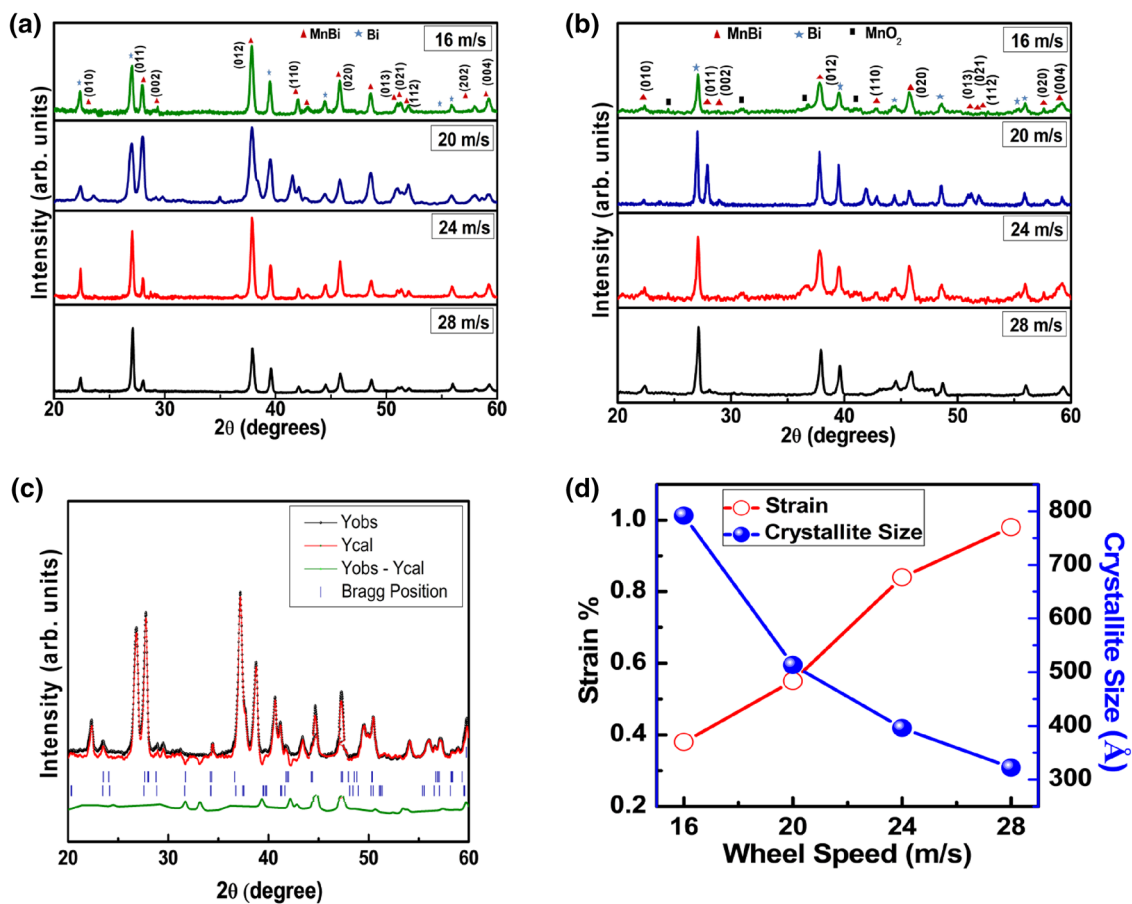
Fig. 3 X-ray diffraction curve of $Mn_{47}Bi_{50}Cr_3$: **a** as-melt-spun ribbons, **b** after ageing for 12 months, at various wheel speeds of 16 m/s, 20 m/s, 24 m/s and 28 m/s. **c** Rietveld refinement of $Mn_{47}Bi_{50}Cr_3$ ribbon, melt spun at a wheel speed of 20 m/s. **d** Variation of strain and the crystallite size with respect to the changing wheel speed for as-melt-spun ribbon

of the samples aged for 12-month duration. There is prevalence of MnO_2 peaks, and the intensity of LTP-MnBi peak has decreased drastically, in agreement with the DSC data. As can be seen from Fig. 3b, the LTP-MnBi peak is well preserved for the sample melt spun at 20 m/s, implying that this is the optimum wheel speed for the formation of a stable LTP-MnBi alloy. Rietveld refinement of $Mn_{47}Bi_{50}Cr_3$ ribbon, melt spun at an optimised wheel speed of 20 m/s, was also carried out to confirm the phase formation. Rietveld analysis was done taking into consideration two phases, namely MnBi (space group: P63/mmc) and Bi (space group: R-3 m), as shown in Fig. 3c.

The crystallite size as obtained from the Scherrer's formula also decreases with the increasing wheel speed (Fig. 3d). The grain size decreases from 80 to 32 nm for the ribbons melt spun at 16 m/s and 28 m/s, respectively. As can be seen from the figure, grain size decreases with the increasing wheel speed, due to higher rate of cooling induced on the melt. Also, the strain as calculated from Williamson–Hall plot suggests that, with increasing wheel speed, more strain is introduced in the alloy (Fig. 3d). The

average strains of the ribbons with the spinning speeds of 16, 20, 24 and 28 m/s were found to be 0.38%, 0.55%, 0.84% and 0.98%, respectively. For lower wheel speed, i.e. under-quenched condition, there is a formation of inhomogeneous microstructure. On the other hand, for higher wheel speed, i.e. over-quenched condition, larger fractions of amorphous phase are observed [23].

3.4 Morphological characterisation

SEM images of $Mn_{47}Bi_{50}Cr_3$ melt-spun ribbons at various wheel speeds of 16 m/s, 20 m/s, 24 m/s and 28 m/s show the variation of grain size with respect to the changing wheel speed (Fig. 4). Sample melt spun at 16 m/s consists of coarse as well as fine-grained microstructure. Whereas, at wheel speed of 20 m/s and above, grain size was found to decrease, in addition, some flaky particles were also observed. It can also be noticed that faster quenched ribbons have less thickness and a fine grain structure. At higher wheel speed, rapid solidification resulting from the water-cooled copper wheel interface generates

Fig. 4 SEM images of $Mn_{47}Bi_{50}Cr_3$ melt-spun ribbons at various wheel speeds of 16 m/s, 20 m/s, 24 m/s and 28 m/s, showing the effect of varying wheel speed on particle size and morphology
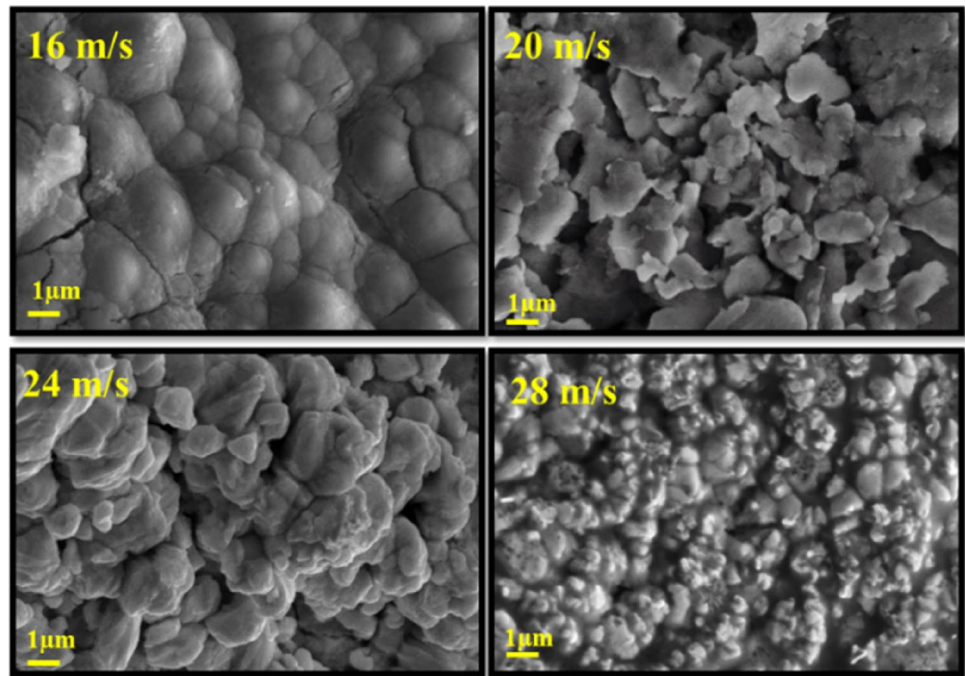
ultra-fine-grained structures with equiaxed grain morphology [24]. As evident from Fig. 4, a decrease in particle size is observed with the increasing wheel speed. This essentially indicates that finer grains are formed at a higher solidification rate. This is in accordance with the previous reports, which states that the grain size varies inversely with the cooling rate and the wheel speed. This is because of the fact that during undercooling, the initial grain size of the ribbon depends on crystal growth rate, heterogeneous nucleation frequency and the time taken for solidification on the surface [25].

3.5 Magnetic characterisation

To study the effect of rate of cooling on the magnetic properties, room-temperature M–H curve was recorded at a maximum applied field of 2 T. As can be seen from Fig. 5a, an increase in magnetisation and coercivity is observed with the increase in wheel speed from 16 m/s to 28 m/s. The maximum increase in coercivity and magnetisation and thereby $(BH)_{max}$ is observed for the sample melt spun at 20 m/s. The value of coercivity and magnetisation for $Mn_{47}Bi_{50}Cr_3$ melt spun at 20 m/s is found to be 11.9 kOe and 54.2 emu/g, respectively, with a $(BH)_{max}$ of 5.1 MGOe. This could be attributed to the optimised cooling rate causing considerable

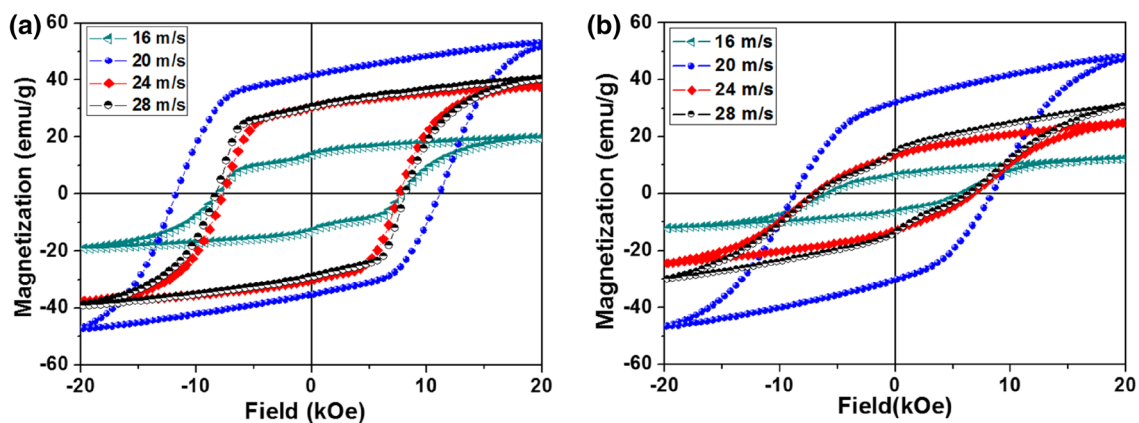**Fig. 5** Room-temperature M–H curve of $Mn_{47}Bi_{50}Cr_3$ melt-spun ribbons at various wheel speeds of 16 m/s, 20 m/s, 24 m/s and 28 m/s: **a** as-prepared, **b** aged 12 months, measured under similar conditions

nucleation leading to fine-grained crystalline microstructure, leading to high value of coercivity.

A high value of coercivity achieved can be attributed to the reduction in grain sizes as seen from SEM images. A decrease in grain size leads to an increase in number of grain boundaries and in turn pinning sites. Also, refinement of grain sizes hinders the nucleation of reverse domains at the grain boundaries and reduces the local demagnetising stray fields. As the grain size approaches single magnetic domain, there is a change in reversal of magnetic domains from domain wall motion to the coherent rotation state. As a consequence of this, a large enhancement in coercivity is observed, due to magnetic isolation of individual grains. This clearly implies that the wheel speed has a significant effect on the microstructure and therefore the magnetic properties. High wheel speed although resulted in higher cooling rates but led to the dominance of undesired phase (such as ferrimagnetic MnBi). On the other hand, lower wheel speeds resulted in very low cooling rates and relatively high grain size in the melt-spun ribbons, resulting in inferior magnetic properties [26]. Thus, optimised wheel speed is therefore essential for obtaining the fine-grained microstructure along with desired magnetic phases.

The evolution and degradation of $Mn_{47}Bi_{50}Cr_3$ sample, aged over 12 months, were also reflected in M–H measurements. As can be seen from Fig. 5b, a decrease in magnetisation and coercivity is observed, due to the oxidation of the samples, as is evident from the DSC curve as well. However, the optimised sample melt spun at 20 m/s and aged for 12 months shows only marginal decrease in its magnetic properties as compared to the other samples.

To further understand the effect of wheel speed on Curie temperature (T_C), magnetisation versus temperature curves were obtained for all four conditions, up to a temperature of 450 °C (Inset of Fig. 6). To precisely determine the value of T_C, derivative of magnetization (dM/dT) was plotted as a function of temperature, for all the four wheel speeds, as shown in Fig. 6. Only a minor change in T_C was observed for samples melt spun at different wheel speeds. The marginal decrease in T_C with the increasing wheel speed may be attributed to the effect of exchange field penetration of the nanocrystalline phase formed during melt spinning, varying with changing wheel speed [27,28].

4 Conclusion

In the current study, the advantages of rapid solidification were utilised to synthesise a more stable Cr-doped MnBi hexagonal phase by optimising the quenching rates, which were controlled by the careful tuning of speed of the water-cooled copper wheel during melt spinning. It was
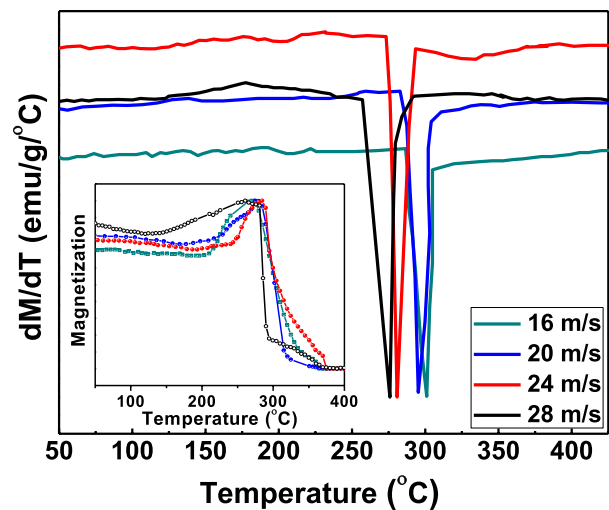

Fig. 6 Determination of Curie temperature of $Mn_{47}Bi_{50}Cr_3$ melt-spun ribbons at various wheel speeds of 16 m/s, 20 m/s, 24 m/s and 28 m/s. Inset: magnetisation versus temperature curve carried out at a constant applied field of 1 kOe

found that the composition $Mn_{47}Bi_{50}Cr_3$ melt spun at an optimised wheel speed of 20 m/s displays high magnetic properties with coercivity 11.9 kOe and magnetisation of 54.2 emu/g. This is attributed to various phenomena such as refined grain structure as studied from SEM images and stable phase formation as deduced from XRD and DSC analysis. In addition to that, the evolution and degradation of the stable LTP-MnBi phase thus formed were also studied through the process of ageing. The samples which were aged for 12 months showed degradation of magnetic properties due to the oxidation of the samples leading to the formation of MnO_2. DSC analysis confirmed the oxidation of samples, except for the sample melt spun at 20 m/s, which further emphasised a more stable phase formation. This study is important from the perspective that melt spinning is a complex yet useful technique which offers maximum solid solubility. And hence, understanding the technique and the optimisation of process parameters is necessary to utilise it to its full potential to enhance the magnetic properties of Cr-doped MnBi alloy. Also, optimisation of melt spinning parameters helps in the direct formation of a stable LTP-MnBi phase, through a single-step reaction, eliminating the need for further annealing. This could serve as a benefit for the production of MnBi-based alloys, which are the ideal candidate for rare-earth free permanent magnet materials.

References

1. J.M.D. Coey, IEEE Trans. Magn. **47**, 4671 (2011)
2. N.V.R. Rao, A.M. Gabay, W. Li, G.C. Hadjipanayis, J. Phys. D: Appl. Phys. **46**, 265001 (2013)
3. N.V.R. Rao, A.M. Gabay, G.C. Hadjipanayis, J. Phys. D: Appl. Phys. **46**, 062001 (2013)
4. X. Guo, X. Chen, Z. Altounian, J.O. Ström-Olsen, Phy. Rev. B **46**, 14578 (1992)
5. H. Yoshida, T. Shima, T. Takahashi, H. Fujimori, Mater. Trans. JIM **40**(5), 455–458 (1999)
6. X. Guo, A. Zaluska, Z. Altounian, J.O. Ström-Olsen, J. Mater. Res. **5**, 2646 (1990)
7. S. Kim, H. Moon, H. Jung, S.M. Kim, H.S. Lee, H. Choi-Yim, W. Lee, J. Alloys Compd. **708**, 1245 (2017)
8. E.J. Lavernia, T.S. Srivatsan, J. Mater. Sci. **45**, 287–325 (2009)
9. S. Öztürk, K. Icin, B. Öztürk, U. Topal, H.K. Odabaşi, Int. J. Mater. Sci. Appl **6**(5), 241–249 (2017)
10. S. Sarafrazian, A. Ghasemi, M. Tavoosi, J. Magn. Magn. Mater. **402**, 115–123 (2016)
11. K. Simeonidis, C. Sarafidis, E. Papastergiadis, M. Angelakeris, I. Tsiaoussis, O. Kalogirou, Intermetallics **19**, 589–595 (2011)
12. N.V. Rama Rao, G.C. Hadjipanayis, J. Alloys Compd. **616**, 319–322 (2014)
13. N.V.R. Rao, G.C. Hadjipanayis, J. Alloys Compd. **629**, 80–83 (2015)
14. P. Metall, M. Srinivas, B. Majumdar, G. Phanikumar, D. Akhtar, Metall. Mater. Trans. B: Process. Metall. Mater. Process. Sci. **42**, 370–379 (2011)
15. K. Anand, N. Christopher, N. Singh, Appl. Phys. A **125**, 12 (2019)
16. B.P. Bewlay, B. Cantor, Int. J. Rapid Solidif. **2**, 107 (1986)
17. V.I. Tkatch, S.N. Denisenko, O.N. Beloshov, Acta Mater. **45**, 2821 (1997)
18. V.I. Tkatch, A.I. Limanovskii, S.N. Denisenko, S.G. Rassolov, Mater. Sci. Eng. A **323**, 91–96 (2002)
19. S. Saha, R.T. Obermyer, B.J. Zande, V.K. Chandhok, S. Simizu, S.G. Sankar, J.A. Horton, J. Appl. Phys. **91**(10), 8525–8527 (2002)
20. K. Oikawa, Y. Mitsui, K. Koyama, K. Anzai, Mater. Trans. **52**(11), 2032–2039 (2011)
21. M. Srinivas, B. Majumdar, D. Akhtar, A.P. Srivastava, D. Srivastava, J. Mater. Sci. **46**, 616–622 (2011)
22. I. Janotová, P. Švec, I. Maťko, D. Janičkovič, P. Švec Sr, AIP Conf. Proc., **1996**, 020021 (2018)
23. Z.M. Chen, Y. Zhang, G.C. Hadjipanayis, Q. Chen, B.M.J. Ma, J. Magn. Magn. Mater. **206**, 8–16 (1999)
24. S. Muthiah, R.C. Singh, B.D. Pathak, P.K. Avasthi, R. Kumar, A. Kumar, A.K. Srivastava, A. Dhar, Nanoscale **10**, 1970–1977 (2018)
25. G. Ouyang, B. Jensen, W. Tang, K. Dennis, C. Macziewski, S. Thimmaiah, Y. Liang, J. Cui, AIP Adv. **8**, 056111 (2018)
26. A.L. Greer, Mater. Sci. Eng. A **133**, 16 (1991)
27. T. Gheiratmand, H.R.M. Hosseini, P. Davami, M. Mansouri, in *4th International Conference on Ultrafine Grained and Nanostructure Matherials* (2018)
28. D.A. Babu, A.P. Srivastava, B. Majumdar, D. Srivastava, D. Akhtar, Metall. Mater. Trans. A **41**(5), 1313–1320 (2010)